



## FULL PAPER

# Efficient synthesis of $\beta$ -aminoketones catalyzed by $\text{Fe}_3\text{O}_4$ @quillaja saponin/Ni (II) as a novel magnetic nano-catalyst

Majid Heidarpour<sup>1</sup> | Hossein Anaraki-Ardakani<sup>2</sup> | Neda Hasanzadeh<sup>1</sup> | Ayeh Rayatzadeh<sup>1</sup>

<sup>1</sup>Department of Chemistry, Ahvaz Branch, Islamic Azad University, Ahvaz, Iran

<sup>2</sup>Department of Chemistry, Mahshahr Branch, Islamic Azad University, Mahshahr, Iran

**Correspondence**

Hossein Anaraki-Ardakani, Department of Chemistry, Mahshahr Branch, Islamic Azad University, Mahshahr, Iran.  
Email: hosseinanaraki@yahoo.com

A new nano-magnetic core-shell  $\text{Fe}_3\text{O}_4$ @quillaja saponin/Ni (II) was synthesized and characterized thoroughly using various tests including energy-dispersive X-ray spectroscopy (EDS), Brunauer–Emmett–Teller (BET), thermo-gravimetric analysis (TGA), high-resolution transmission electron microscopy (HR-TEM), vibrating sample magnetometer (VSM), Fourier transform infrared (FT-IR) spectroscopy, inductively coupled plasma (ICP), X-ray diffraction (XRD) and scanning electron microscopy (SEM). The achievements demonstrated that the proposed agents were beneficial to synthesis the derivatives of  $\beta$ -aminoketone. Moreover, it was possible to recover the catalyst by means of simple magnetic decantation quickly. Besides, no reduction in the activity of the catalyst occurred, even though it was utilized in various reactions.

**KEYWORDS**

green chemistry, nano  $\text{Fe}_3\text{O}_4$ , nickel (II) chloride, quillaja saponin, three-component

## 1 | INTRODUCTION

Considering specific merits of heterogeneous catalysts, many research activities have been made in recent years by chemists to utilize this catalyst. Easy storage, as well as easy handling, and also the ability to be recovered and reproduced in an easy way, can be mentioned as some of their advantages.<sup>[1,2]</sup> A big section of these catalysts is profound intractable the supporting material, and thus reactants have finite accessibility to the catalytic sites.<sup>[3]</sup> But with the use of nanometer scales, the energetic level of these catalysts increases and can be completely dispersed in solutions and produce homogeneous conditions.<sup>[4,5]</sup>

In this area, MNPs are known as efficient nano-support because they are recovered from the mixture by a magnet, which is more convenient and efficient than the filtration or centrifugation approach. In recent years,  $\text{Fe}_3\text{O}_4$  MNPs have been utilized commonly as

a heterogeneous MNPs support for organic-based catalysts.<sup>[6,7]</sup> Among different nanoparticles,  $\text{Fe}_3\text{O}_4$  nanoparticles widely studied by researchers as the core magnetic support owing to its specific properties such as strong magnetic properties, high chemical stability, being abundant, effortless preparation via coprecipitation, and low toxicity.<sup>[8,9]</sup> It should be noted that pure  $\text{Fe}_3\text{O}_4$  nanoparticles, with the high surface area to volume ratio, are highly chemically active and suffer from an inherent instability.<sup>[10]</sup> They are very sensitive to oxidation and tend to aggregate spontaneously when exposed to acids and aqueous solutions. In order to surmount these limitations, it is essential to protect the surface of nanoparticles by an external layer made out of carbon and silica.<sup>[11,12]</sup>

Recently, many researchers try is to produce catalysts by covering magnetic nanoparticle iron oxide with organic materials initiate in plants. The Licorice plant, Quillaja Saponaria (saponin), is one of those

organic materials which are a huge evergreen plant with leathery and bright leaves. They also have thick bark and are originally from Peru, China, and the semi-arid regions of Chile.<sup>[13]</sup> Generally, sapogenin widely found in terrestrial plants like the bark of quillaja and marine animals. Investigating the chemical structure of sapogenin is concluded in that sapogenins are steroids having extremely broad applications related to cancer, blood circulation system, and some other clinical issues.<sup>[14–16]</sup> Sapogenin used in industry is provided from the outer layer quillaja trunk.

In recent years, extracts of natural plants have extensively exploited as foam-making materials in beverages, emulsifiers in food and Medicine, and soaking agents in photography.<sup>[17]</sup> Sapogenin is dominantly composed of cellulose, a part of which is hydrophobic, the other part is hydrophilic. Functional groups existing in the hydrophilic part of the sapogenin make it capable of chemical modifications. Therefore, sapogenin can be used in order to bond various functional groups to synthesis polymeric catalysts.<sup>[18]</sup>

Among the family of cellulose derivatives, the building of the quillaja sapogenin (QS) in particular is appealing because it contains a mixture of major properties of quillaja sapogenin with incredible features of materials. Owing to the presence of OH groups in its polymeric tissue, it will be applied as an effective coating for iron nanoparticles, and then obtained by engaging an active metal halide at the Core-shell surface.<sup>[19]</sup>

Munnich type reactions were conducted to form C-C bonds in the synthesis process. Compounds of the  $\beta$ -aminoketones, which are necessary intermediates in herbal products, were provided through the mentioned process.<sup>[17,20]</sup>

Previously, a portion of the  $\beta$ -aminoketone's compounds had already been catalyzed by  $H_3PW_{12}O_{30}$  (hetero poly acids),<sup>[21]</sup> carbon-based solid acid,<sup>[22]</sup> diaryliodonium (III),<sup>[23]</sup>  $BiNO_3$ ,<sup>[24]</sup> citric acid,<sup>[25]</sup> proline and solution,<sup>[26,27]</sup> calixarenes,<sup>[28]</sup>  $Cu/NH_2$ -SBA-15,<sup>[29]</sup>  $InCl_3$ <sup>[30]</sup> ionic liquid (carboxyl-functionalized poly) (CFPIL).<sup>[31]</sup> The mentioned catalysts for this purpose, despite having some advantages, have also some disadvantages, including time consuming reaction process, a small yield of products, harmfulness, and low efficiency in the recovery process. Thus, it seems essential to replace them with other ones without owing to these disadvantages.

In this report, we synthesis and characterize nano- $Fe_3O_4@Qs/Ni$  (II) as a bio-based, magnetic, and effective heterogeneous catalyst for the synthesis of  $\beta$ -aminoketones.

## 2 | EXPERIMENTAL

### 2.1 | General

All chemicals utilized in this work were provided from Aldrich and Merck companies and used without further purification. An electrothermal apparatus was implemented to measure the melting points of utilized chemicals in the laboratory. FT-IR spectra were detected in a range between 4,000 and 400  $cm^{-1}$  by Perkin Elmer apparatus. In order to monitor the progress of reactions, thin-layer chromatography (TLC) test was conducted under UV light to visualize the process well enough. TLC papers were provided in Merck. A Philips XRD apparatus was utilized to analyze the powder of product via  $Cu/K\alpha$  radiation, the wavelength of which was 1.54 Å.

TGA experiments were done by a LINSEIS MODEL 1600 PT. The apparatus is commonly used for thermal analysis purposes with a heating rate of 5 °C/min under ambient pressure. The magnetic properties of the sample were identified through vibrating sample magnetometer under room temperature.

$^1H$  and  $^{13}C$  NMR spectra were studied by a Bruker DRX-500 Avance spectrometer. DMSO- $d_6$  solution by TMS was utilized as the internal standard. A Mira III apparatus was implemented to obtain SEM. EDX analysis was performed for the mapping of the nanocomposites elements. It should be mentioned that a 10 mA layer of gold was utilized to cover the surface of the sample two minutes before the test.

## 3 | METHODS

### 3.1 | $Fe_3O_4$ MNPs preparation

MNPs precipitated in the alkali solution of Fe (III) and Fe (II) (molar ratio 2:1) at 80 °C via the standard coprecipitation method reported by Liu et al.<sup>[32]</sup>

$FeCl_3 \cdot 6H_2O$  (10 mmol, 2.7 g) and  $FeSO_4 \cdot 7H_2O$  (10 mmol, 1.39 g) were gradually poured in a 100 ml sample of distilled water, which had already been deoxygenated. The mixture was vigorously dispersed at 80 °C under nitrogen gas protection. Afterward, a 7.5 mm sample of ammonium hydroxide was added to the dispersed mixture swiftly.

The reaction mixture was suddenly incorporated with ammonium hydroxide by a volume of 7.5 ml. Finally, the base was added to the aqueous phase of  $Fe^{2+}/Fe^{3+}$  forming black precipitations, which were MNPs. The process was preceded for another 1 hr, and the aqueous phase was cooled down to ambient temperature. Black precipitations were isolated via an external magnet. After

gathering them from the aqueous phase, they were washed by water and dried in a vacuum 4 times.<sup>[33,34]</sup>

### 3.2 | Preparation of nano-Fe<sub>3</sub>O<sub>4</sub>@ Quillija Saponin

A mixture of synthesized nano-Fe<sub>3</sub>O<sub>4</sub> (1.5 g) and Quillaja Saponin (2.5 g) in 30 ml ethanol was stirred for 20 min at ambient temperature. After the reaction, the products were removed by a magnet and dried at room temperature, 3.96 g of product were obtained.

### 3.3 | Preparation of nano-Fe<sub>3</sub>O<sub>4</sub>@ Quillija Saponin/Ni (II)

The obtained nano-Fe<sub>3</sub>O<sub>4</sub> powder (0.15 g) and quillaja saponin (0.3 g) and NiCl<sub>2</sub>·6H<sub>2</sub>O (1 g) were dispersed in an ethanol sample (10 ml) via stirrer at ambient temperature for half of an hour. After the reaction, the solvent was evaporated at room temperature to be obtained in good yields. Afterward, its magnetic properties were analyzed. In the next step, products were washed via ethanol again.

### 3.4 | β-aminoketones' synthesizing procedure

A mixture of aromatic aldehydes (1 mmol), amines (1 mmol), ketones (1.1 mmol), and nano-Fe<sub>3</sub>O<sub>4</sub>@Qs/Ni (II) (0.07 g) was mixed in EtOH (15 ml) at room conditions. After the end of the reaction, which was recognized by TLC, the synthesized catalyst was gathered with a magnet, and the mixture was then warmed to achieve the crude product. Finally, the crude product was purified by ethanol/acetone crystallization; the following compounds were achieved.

Spectral data of the purified products **4 h-m**.

### 3.5 | 3-(4-Bromo-phenylamino)-1,3-diphenyl-propan-1-one (Table 3, entry 4 h)

Mp 177–179 °C, IR (KBr, cm<sup>-1</sup>): 768, 858, 1,067, 1,311, 1,515, 1,606, 1,677, 2,888, 3,412. Analyses: Calcd, For C<sub>21</sub>H<sub>18</sub>BrNO: C, 66.33; H, 4.77; N, 3.68; O, 4.21%. Found: C, 66.36; H, 4.80; N, 3.64%. <sup>1</sup>H NMR(300 MHz, CDCl<sub>3</sub>): δ = 7.97–6.61(m,14H), 6.35(d, J = 6 Hz, 1H), 5.11(m, 1H), 3.54(m, 2H). (<sup>13</sup>CNMR, 75 MHz, CDCl<sub>3</sub>): δ = 198.1, 146.9, 141.6, 137.9, 133.1, 131.9, 128.6, 128.43, 128.4, 127.6, 126.1, 116.9, 116.8, 55.14, 44.5 ppm.

### 3.6 | 3-(4-Bromo-phenylamino)-3-(4-chloro-phenyl)-1-phenyl-propan-1-one (Table 3, entry 4i)

Mp 171–173 °C, IR (KBr, cm<sup>-1</sup>): 751, 1,082, 1,300, 1,511, 1,599, 1,682, 3,376; Analyses: Calcd, For C<sub>21</sub>H<sub>17</sub>BrClNO: C, 60.82; H, 4.13; N, 3.38; Found: C, 60.87; H, 4.17; N, 3.31%. <sup>1</sup>H NMR(300 MHz, CDCl<sub>3</sub>): δ = 7.92(s, 2H), 7.87(d, J = 1.4 Hz, 1H), 7.58(m, 2H), 7.46(t, J = 7.82 Hz, 2H), 7.38–7.27(m, 2H), 7.19–7.15(m, 2H), 6.43–6.40(m, 2H), 4.92(br, 1H), 4.65(s, br, 1H), 3.45(m, 2H). (<sup>13</sup>CNMR, 75 MHz, CDCl<sub>3</sub>): δ = 197.8, 145.7, 140.9, 136.4, 133.7, 133.2, 131.8, 129.05, 128.8, 128.1, 127.7, 115.4, 109.8, 54.2, 44.9 ppm.

### 3.7 | 3-(4-Bromo-phenylamino)-1-phenyl-3-p-tolyl-propan-1-one (Table 3, entry 4j)

Mp 175–177 °C, IR (KBr, cm<sup>-1</sup>): 761, 1,092, 1,312, 1,398, 1,513, 1,603, 1,673, 3,060, 3,395; Analyses: Calcd, For C<sub>22</sub>H<sub>20</sub>BrNO: C, 67.01; H, 5.11; N, 3.55%; Found: C, 67.11; H, 5.18; N, 3.58%; <sup>1</sup>H NMR (300 MHz, CDCl<sub>3</sub>): δ = 7.94–6.43(m, 13H), 6.40(m, 1H), 4.91(m, 1H), 3.60(d, d, J = 12, J = 4.5 Hz, 1H), 3.34–3.22(d, d, J = 12, J = 4.5 Hz, 1H), 2.23(s, 3H). (<sup>13</sup>CNMR, 75 MHz, CDCl<sub>3</sub>): δ = 198.5, 136.1, 134.8, 129.84, 129.80, 129.6, 129, 128.9, 128.7, 128.1, 127.8, 120.8, 114, 54.4, 46.4, 21 ppm.

### 3.8 | 3-(4-nitro-phenylamino)-1-phenyl-3-p-tolyl-propan-1-one (Table 3, entry 4 k)

Mp 163–165 °C, IR (KBr, cm<sup>-1</sup>): 767, 861, 1,223, 1,313, 1,513, 1,599, 1,670, 3,026, 3,391; Analyses: Calcd, For C<sub>22</sub>H<sub>20</sub>N<sub>2</sub>O<sub>3</sub>: C, 73.32; H, 5.59; N, 7.77%; Found: C, 73.38; H, 5.51; N, 7.81%; <sup>1</sup>H NMR (300 MHz, CDCl<sub>3</sub>): δ = 7.98–6.58(m, 13H), 5.12(m, 1H), 4.35(s, 1H), 3.72(m, 1H), 3.39(m, 1H), 2.24(s, 3H). (<sup>13</sup>CNMR, 75 MHz, CDCl<sub>3</sub>): δ = 197.85, 152.2, 138.2, 138, 137.6, 135.25, 129.75, 128.8, 128.4, 128.15, 127.7, 126.6, 112.1, 53.9, 45.55, 21.05 ppm.

### 3.9 | 4-(4-Bromo-phenyl)-1,3-diphenyl-4-phenylamino-butan-2-one (Table 3, entry 4 l)

Mp 124–126 °C, IR (KBr, cm<sup>-1</sup>): 658, 703, 753, 1,504, 1,605, 1,707, 3,436; Analyses: Calcd, For C<sub>28</sub>H<sub>24</sub>BrNO: C, 71.49; H, 5.14; N, 2.98% Found: C, 71.58; H, 5.29; N, 2.78%, <sup>1</sup>H NMR (300 MHz, CDCl<sub>3</sub>) δ = 7.36–7.17 (m, 10 H), 6.97–6.94 (m, 4H), 6.75–6.5 (m, 3H), 6.29 (d, J = 7.67 Hz, 2H), 4.94 (d, Anti, J = 9.97 Hz, 0.92 H), 4.85

(d, syn,  $J = 4.81$  Hz, 0.08 Hz), 4.13 (d, syn,  $J = 7.3$  Hz, 0.09 H), 4.09 (d, anti,  $J = 10.16$  Hz, 0.91 H), 3.73 (s, br, 1H), 3.39 (s, 2H). ( $^{13}\text{C}$ NMR, 75 MHz,  $\text{CDCl}_3$ ):  $\delta = 204.7$ , 146.8, 141.15, 134.3, 132.6, 131.6, 129.6, 129.4, 129.1, 128.9, 128.7, 128.5, 127, 121.2, 118.1, 113.9, 113.5, 64.4, 58.9, 50.45 ppm.

### 3.10 | 4-(4-Chloro-phenyl)-1,3-diphenyl-4-phenylamino-butan-2-one (Table 3, entry 4 m)

Mp 170–171 °C, IR (KBr,  $\text{cm}^{-1}$ ): 684, 700, 759, 1,511, 1,608, 1,705, 3,443; Analyses: Calcd, For  $\text{C}_{28}\text{H}_{24}\text{ClNO}$ : C, 78.95; H, 5.68; N, 3.29% Found: C, 78.78; H, 5.41; N, 3.43%  $^1\text{H}$  NMR (300 MHz,  $\text{CDCl}_3$ )  $\delta = 7.36$ – $7.27$  (m, 7H), 7.2–7.17 (m, 3H), 7.07–6.95 (m, 3H), 6.75 (d,  $J = 1.35$  Hz 1H), 6.72 (d,  $J = 1.89$  Hz, 1H), 6.64–6.58 (m, 1H), 6.37 (d,  $J = 7.6$  Hz, 1H), 6.30 (d,d,  $J = 8$ ,  $J = 0.83$  Hz, 2H), 4.97 (d, anti,  $J = 10.15$  Hz, 0.82H), 4.86 (d, syn,  $J = 7.4$  Hz 0.18H), 4.49 (s, br, 1H), 4.11 (d, syn,  $J = 7.4$  Hz, 0.18H), 4.08 (d, anti,  $J = 10.15$  Hz, 0.82H), 3.39 (s, 2H). ( $^{13}\text{C}$ NMR, 75 MHz,  $\text{CDCl}_3$ ):  $\delta = 204.8$ , 146.8, 140.6, 134.3, 132.6, 131.6, 129.6, 129.4, 129.1, 128.9, 128.7, 128.5, 127, 121, 117.7, 113.9, 113.65, 64.4, 58.9, 50.5 ppm.

## 4 | RESULTS AND DISCUSSION

Nano- $\text{Fe}_3\text{O}_4$ @Qs/Ni (II) was prepared through a two-step process. The first step was synthesis of nano- $\text{Fe}_3\text{O}_4$  by

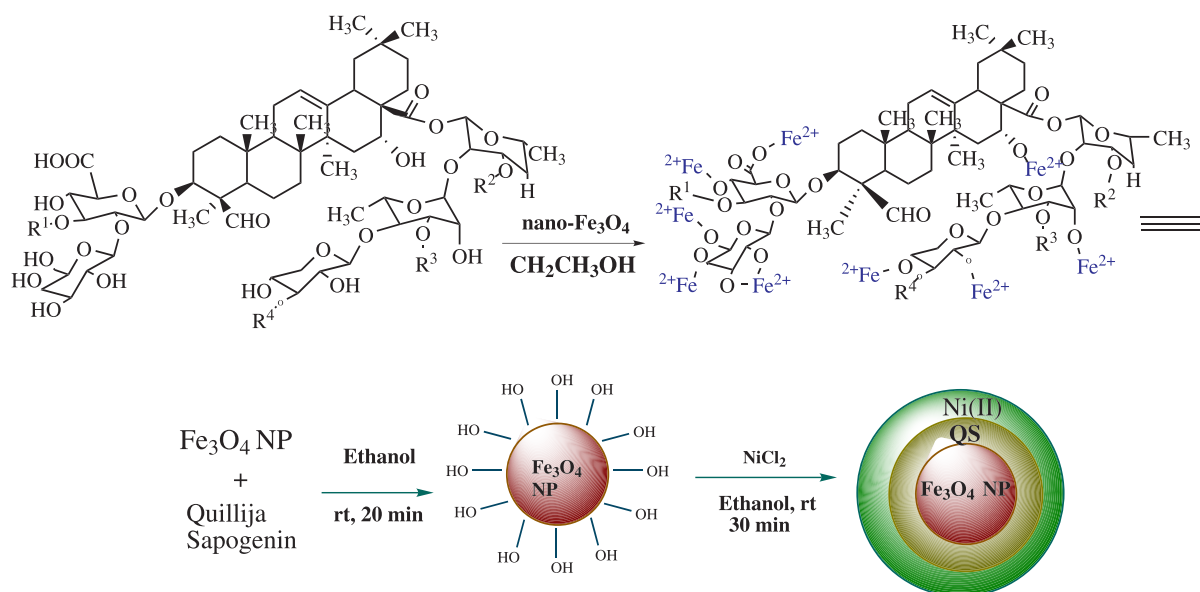
$\text{Fe}^{2+}$  and  $\text{Fe}^{3+}$  ions' co-precipitation, and then the product of the first step was stirred with Quillaja Sapogenin. Afterwards, it was utilized as a magnetic support in order to bond  $\text{NiCl}_2$  (Scheme 1).

The synthesized catalyst, nano- $\text{Fe}_3\text{O}_4$ @Qs/Ni (II), is characterized by FT-IR (Fourier transform infrared spectroscopy), XRD (X-ray diffraction), VSM (vibrating sample magnetometer), ICP (inductively coupled plasma), EDX (Energy-dispersive X-ray spectroscopic analysis), BET (Brunauer–Emmett–Teller), SEM (scanning electron microscopy), HR-TEM (high-resolution transmission electron microscopy), and TGA (thermogravimetric analysis).

The results obtained from FT-IR spectroscopy of (A) nano- $\text{Fe}_3\text{O}_4$ , (B) nano- $\text{Fe}_3\text{O}_4$ @Qs, (C) nano- $\text{Fe}_3\text{O}_4$ @Qs/Ni(II) are presented in Figure 1. An intensive band observed in  $585\text{ cm}^{-1}$  through FT-IR spectra of the nano- $\text{Fe}_3\text{O}_4$  disclosed the presence of Fe-O stretching vibrations. Furthermore, the wideband between 3,300 and  $3,500\text{ cm}^{-1}$  is an indication of the presence of the O-H bond stretching vibration.

Presence of Fe-O stretching vibration regarding the absorption of nano- $\text{Fe}_3\text{O}_4$ @Qs, Quillija Sapogenin (B) indicates that Quillija Sapogenin covers the magnetic nano- $\text{Fe}_3\text{O}_4$ . Wideband at  $3383\text{ cm}^{-1}$ , which has resulted from the presence of OH group, in conjunction with the absorption bands around  $2,925\text{ cm}^{-1}$  illustrates the stretching vibrations of the C-H bonds. A band at  $1619\text{ cm}^{-1}$  denotes to the bending vibrations of H-O-H. The absorption band between 1,065 and  $1,100\text{ cm}^{-1}$  illustrates the existence of the C-O bonds.

The FT-IR spectra of the nano- $\text{Fe}_3\text{O}_4$ @Qs/Ni (II) (C) demonstrate a band at  $415\text{ cm}^{-1}$  that can be



**SCHEME 1** Preparation of nano- $\text{Fe}_3\text{O}_4$ @Qs/Ni (II)

corresponded by O–Ni–O bending vibrations. The band at  $615\text{ cm}^{-1}$  correspondings to stretching vibrations of Fe–O groups. The  $1,626\text{ cm}^{-1}$  band demonstrates the presence of H–O–H bending vibrations. Bands around  $2,921\text{ cm}^{-1}$  refer to the stretching vibration of C–H, the stretching vibrations of O–H bonds have been recognized at  $3375\text{ cm}^{-1}$ .

In comparison with nano- $\text{Fe}_3\text{O}_4$ @Qs, bonding Ni (II) to the Qs shifts Fe–O stretching vibrations to lower wave range (from  $626\text{ cm}^{-1}$  to  $615\text{ cm}^{-1}$ ) (Figure 1).

Structure and purity of the nano- $\text{Fe}_3\text{O}_4$  (A), nano- $\text{Fe}_3\text{O}_4$ @Qs (B), and nano- $\text{Fe}_3\text{O}_4$ @Qs/Ni (II)(C) are

studied by means of high angle X-ray diffraction analysis (XRD) (Figure 2).

The bare  $\text{Fe}_3\text{O}_4$  illustrates peaks at  $2\theta = 30.3832^\circ$ ,  $35.7926^\circ$ ,  $42.7498^\circ$ ,  $52.6881^\circ$ ,  $56.3598^\circ$ ,  $61.64866^\circ$  with FWHM equal to 0.4722, 0.4722, 0.4723, 0.7873, 0.6298 and 0.6298 demonstrates the cubic structure of the high-pure  $\text{Fe}_3\text{O}_4$  explained by other researchers (Figure 2A).<sup>[40]</sup>

The same peaks were obtained from the XRD pattern of nano- $\text{Fe}_3\text{O}_4$ @Qs, which illustrates the preservation of the structure of the crystalline spinel ferrite core while cellulose coating process.

**FIGURE 1** FT-IR spectra of (a) nano- $\text{Fe}_3\text{O}_4$ , (b) nano- $\text{Fe}_3\text{O}_4$ @Qs, (c) nano- $\text{Fe}_3\text{O}_4$ @Qs/Ni (II)

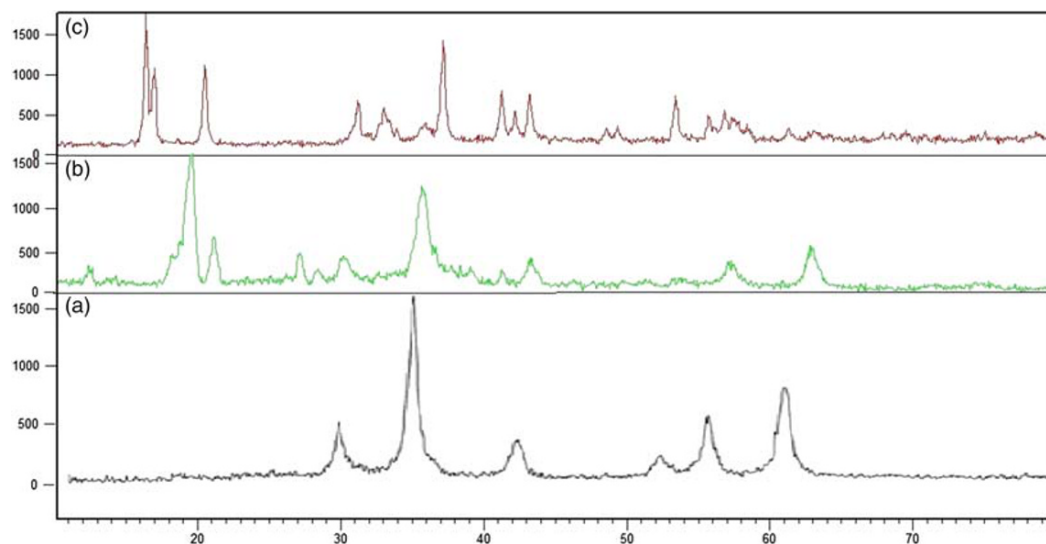
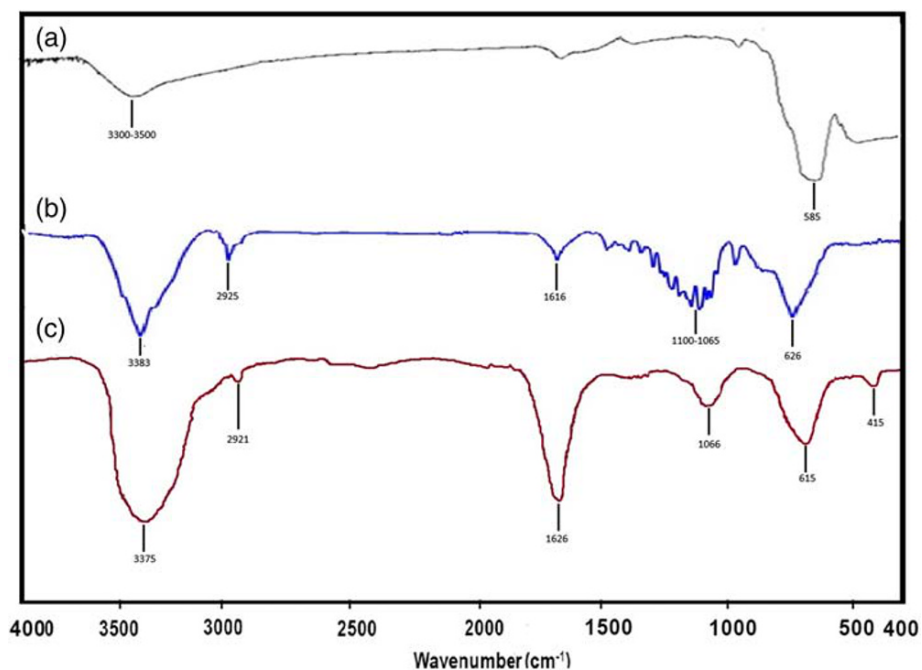


**FIGURE 2** XRD patterns of the (a) nano- $\text{Fe}_3\text{O}_4$ , (b) nano- $\text{Fe}_3\text{O}_4$ @Qs, (c) nano- $\text{Fe}_3\text{O}_4$ @Qs/Ni (II)

Furthermore, other peaks at  $2\theta = 19.8^\circ$  and  $21.3^\circ$ , denote to the sapogenin cover on nano- $\text{Fe}_3\text{O}_4$  (Figure 2 B). The XRD outputs of nano- $\text{Fe}_3\text{O}_4@Qs/Ni$  (II) are an indication of the amorphous structure.

Peaks observed at  $2\theta = 12.5^\circ$ ,  $19^\circ$ ,  $21^\circ$ ,  $27^\circ$  were also observed in the  $\text{Fe}_3\text{O}_4@Qs$  (Figure 2. C). The diffraction peaks at  $2\theta = 16.6^\circ$ ,  $49.1^\circ$ ,  $53.6^\circ$ ,  $55.73^\circ$  demonstrate the  $\text{NiCl}_2$  core. A sharp peak around  $2\theta = 37$  indicates the existence of nano- $\text{Fe}_3\text{O}_4@Qs$  and bonding of Ni to Qs shell.

Thermo-gravimetric analysis (TGA) has been conducted at temperatures between 0 to  $800^\circ\text{C}$  (Figure 3). (A) illustrates TGA data of nano- $\text{Fe}_3\text{O}_4@Qs$ . The curve indicates three phases of mass-loss. Firstly, the mass loss occurred from 20 to  $135^\circ\text{C}$  was very low (about 12.64%) and was related to inter-crystalline water and solvents' vapor. The second and third steps refer to the mass loss resulted from weight loss due to the decomposition of quillaja sapogenin molecules from the formation of cellulose compounds. In the second step, 35.27% mass loss was observed in temperatures between 170 and  $510^\circ\text{C}$ . The third mass loss occurred from  $640^\circ\text{C}$  to  $800^\circ\text{C}$ .

The TGA (B) is related to nano- $\text{Fe}_3\text{O}_4@Qs/Ni$  (II). The curve shows two mass-loss steps. Firstly, a weight loss (39.49%) from  $90^\circ\text{C}$  to  $416^\circ\text{C}$  is related to the removal of moisture and solvent and some organic compounds of the catalyst. Subsequently, and other weight loss steps, the main weight loss (39.85%) from  $422^\circ\text{C}$  to

$800^\circ\text{C}$  is related to metals and some organic compounds (Figure 3).

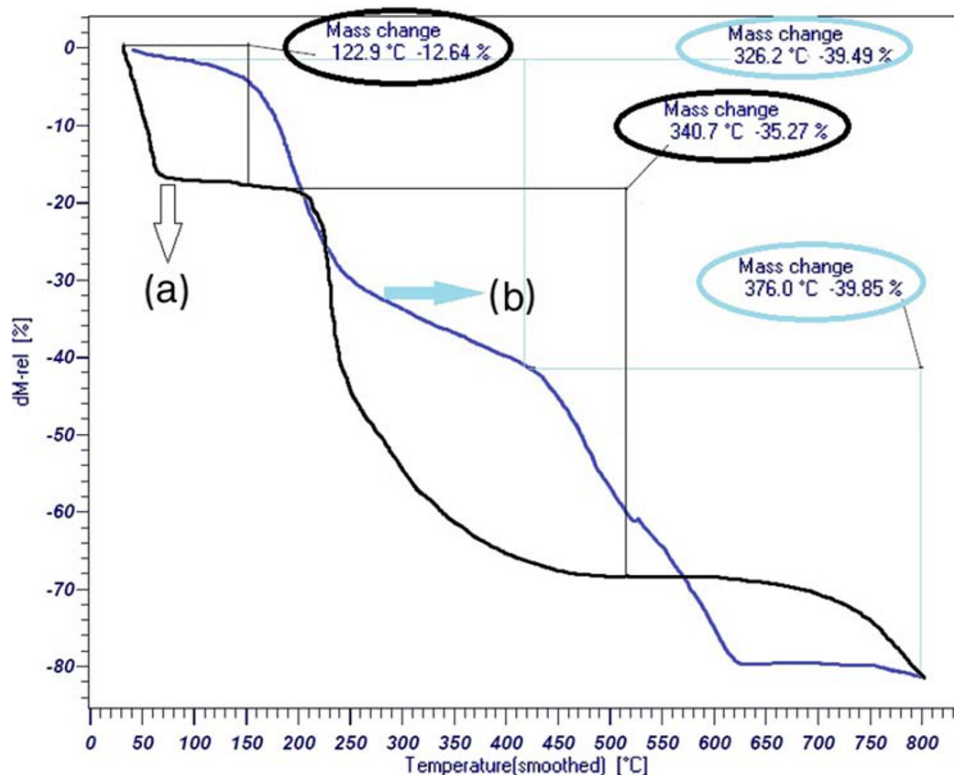
To evaluate the elemental concentration of nano- $\text{Fe}_3\text{O}_4@Qs$ , an EDS test was performed. As shown in Figure 4, the results of EDS nano  $\text{Fe}_3\text{O}_4@Qs$  demonstrate the existence of C, Fe, and O. Moreover; EDS experiment outputs confirmed that the nano-  $\text{Fe}_3\text{O}_4$  and quillaja were combined (Figure 4).

The presence of the desired elements in nano- $\text{Fe}_3\text{O}_4@Qs/Ni$  (II) was approved by EDX analysis (energy-dispersive X-ray spectroscopy) (Figure 5). EDX outputs obviously confirmed the existence of Fe, Cl, Ni, O, C elements in the synthesized catalyst.

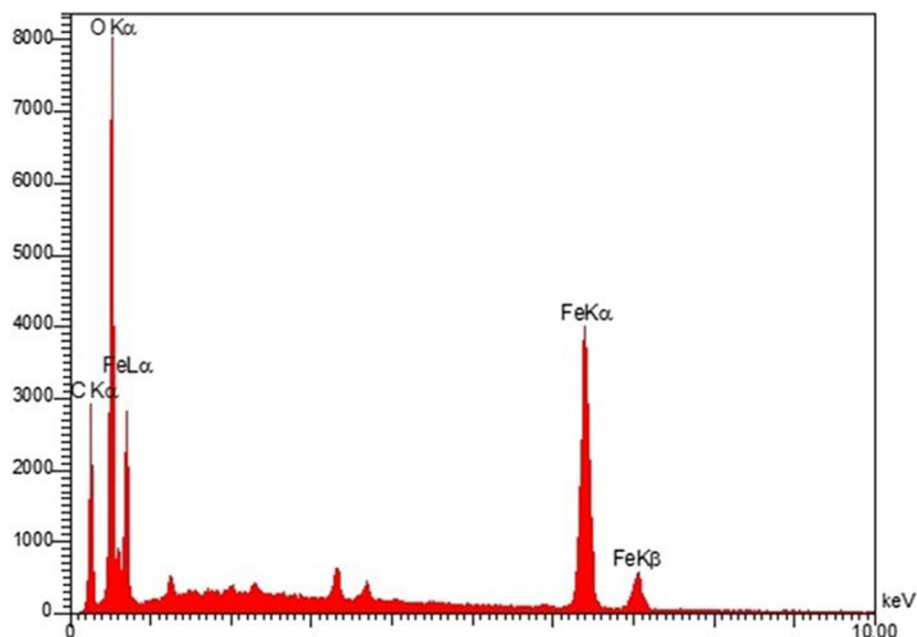
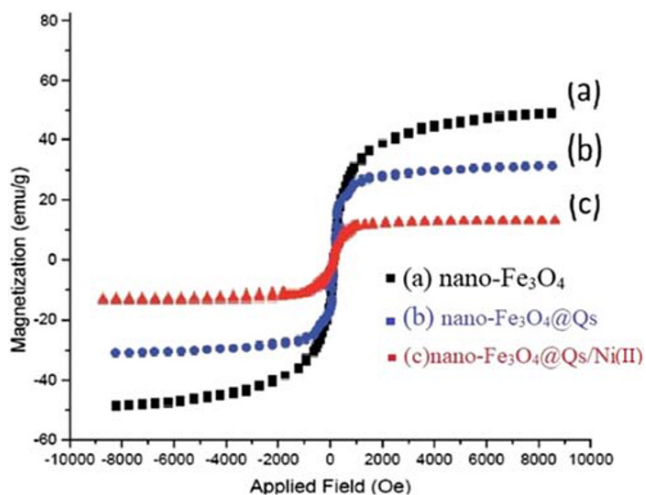
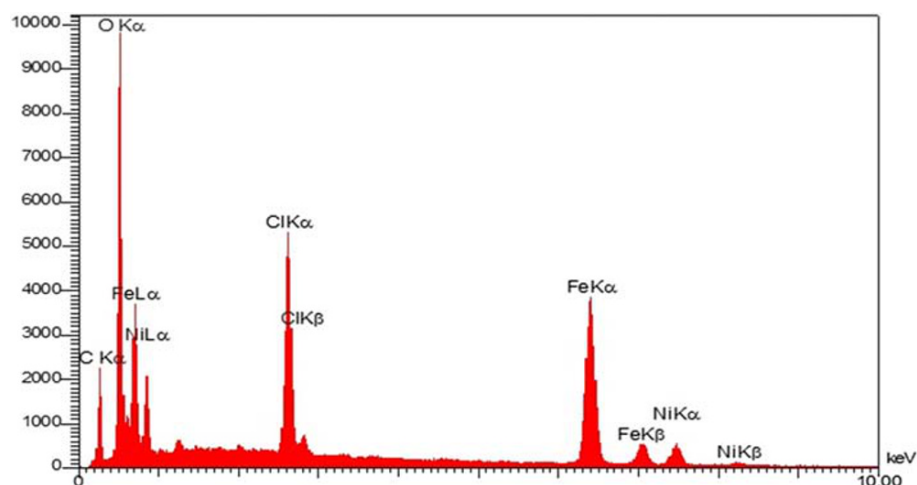
The magnetic characteristics of the nano- $\text{Fe}_3\text{O}_4$  (A), nano- $\text{Fe}_3\text{O}_4@Qs$  (B), and nano- $\text{Fe}_3\text{O}_4@Qs/Ni$  (II) were evaluated at ambient temperature by a VSM analysis, which is presented in Figure 6.

The whole of the results shows superparamagnetic behavior. Therefore, the saturation magnetization of nanoparticles is approximately  $70.0\text{ emu/g}$  (Figure 6a) and is far less than its bulk counterparts ( $92.0\text{ emu/g}$ ).<sup>[41–44]</sup> The nano- $\text{Fe}_3\text{O}_4@Qs/Ni$  (II) magnetization was lower than  $30.0\text{ emu/g}$ . This might result from the presence of a Sapogenin and Ni shells as double layers around nano- $\text{Fe}_3\text{O}_4$  core.

The morphology and size of the nano- $\text{Fe}_3\text{O}_4@Qs/Ni$  (II) were investigated by scanning electron microscopy (SEM). indicates that the dimensions of nano- $\text{Fe}_3\text{O}_4@Qs/Ni$  (II) are between 21 and 44 nm (Figure 7).



**FIGURE 3** Thermal gravimetric analysis pattern of (a) nano- $\text{Fe}_3\text{O}_4@Qs$ , (b) nano- $\text{Fe}_3\text{O}_4@Qs/Ni$  (II)

**FIGURE 4** EDS diagram of nano-Fe<sub>3</sub>O<sub>4</sub>@Qs**FIGURE 5** EDS diagram of nano-Fe<sub>3</sub>O<sub>4</sub>@Qs/Ni (II)**FIGURE 6** Magnetization loops of (a) nano-Fe<sub>3</sub>O<sub>4</sub>, (b) nano-Fe<sub>3</sub>O<sub>4</sub>@Qs and (c) nano-Fe<sub>3</sub>O<sub>4</sub>@Qs/Ni (II)

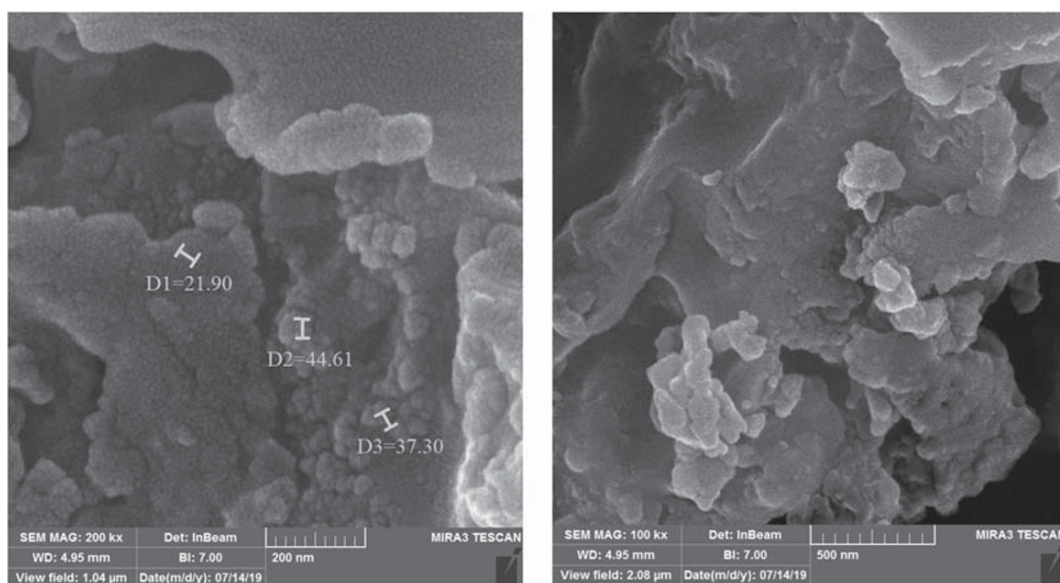
HR-TEM images were prepared to study the morphological characteristics of the catalyst, which are illustrated in Figures 8a and b.

HR-TEM test results convey the message that the shape of Fe<sub>3</sub>O<sub>4</sub>@Qs/Ni (II) MNPs is a sphere with a size range between 21 and 44 nm. Images shown in Figure 8 illustrates that a layer of Qs with a thickness of 8 nm is formed around Fe<sub>3</sub>O<sub>4</sub> MNPs as a core-shell after being modified by Qs.

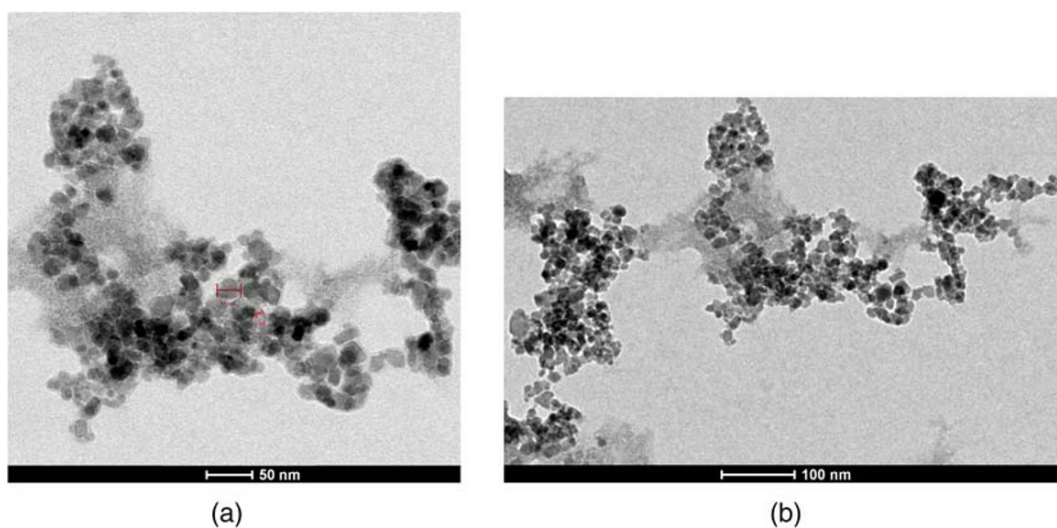
Furthermore, based on Figure 8, the average diameter for Fe<sub>3</sub>O<sub>4</sub>@Qs/Ni (II) is 33 nm.

Figure 9 illustrates the isotherms of N<sub>2</sub> adsorption-desorption on nano-Fe<sub>3</sub>O<sub>4</sub>@Qs and nano-Fe<sub>3</sub>O<sub>4</sub>@Qs/Ni (II).

The catalyst sample classifies as mesoporous materials, according to IUPAC, because it exhibits the IV type behavior. The total surface area of Fe<sub>3</sub>O<sub>4</sub>@Qs was reduced from 8.9317 to 3.1174 m<sup>2</sup> g<sup>-1</sup> after adsorbing



**FIGURE 7** SEM image of synthesized nano-Fe<sub>3</sub>O<sub>4</sub>@Qs/Ni (II)



**FIGURE 8** (a). HR-TEM of synthesized catalyst at 50 nm scale. (b). HR-TEM of synthesized catalyst at 100 nm scale

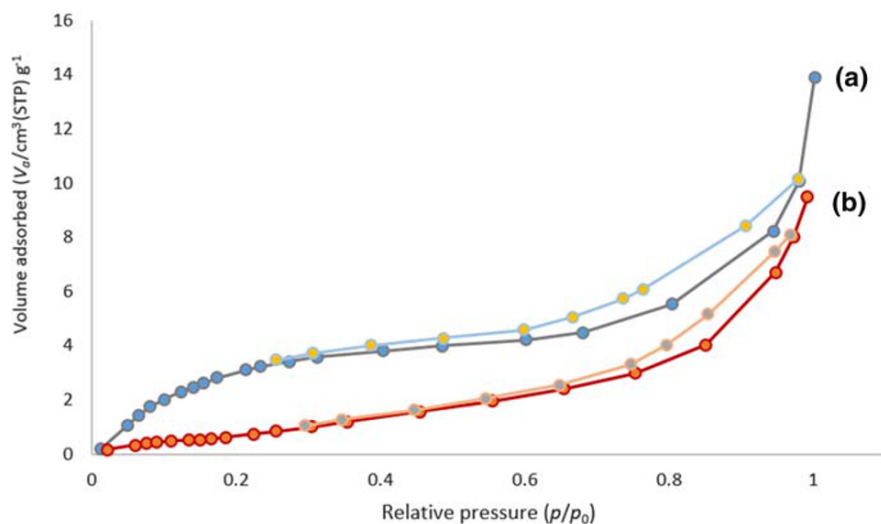


**FIGURE 9** N<sub>2</sub> adsorption–desorption isotherms of nano-Fe<sub>3</sub>O<sub>4</sub>@Qs (a), nano-Fe<sub>3</sub>O<sub>4</sub>@Qs/Ni (II) (b)

Ni. Therefore, it can be said that the decrease in the amount of pore volume results from adsorption on Ni complex on Qs surface. Results obtained from this test show that because of the existence of a high volume of organic materials presents in the inner surface of  $\text{Fe}_3\text{O}_4$  (Figure 9). The surface characteristics of the catalyst are tabulated in Table 1. In order to depict the magnetic characteristics of the prepared catalyst, nano- $\text{Fe}_3\text{O}_4$ @Qs/Ni (II) is dispersed in ethanol, which leads to a dark aqueous phase. By means of an external magnet, the nano- $\text{Fe}_3\text{O}_4$ @Qs/Ni (II) was totally gathered on one side of the container. (Figure 10).

We have examined the catalytic activity of nano- $\text{Fe}_3\text{O}_4$ @Qs/Ni (II) for the preparation of  $\beta$ -aminoketone derivatives via a one-pot three-component reaction

**TABLE 1** Surface properties of nano- $\text{Fe}_3\text{O}_4$ @Qs and nano- $\text{Fe}_3\text{O}_4$ @Qs/Ni (II)

Sample	SBET ( $\text{m}^2/\text{g}$ )	Pore diam by BJH method (nm)	Pore vol ( $\text{cm}^3/\text{g}$ )
Nano- $\text{Fe}_3\text{O}_4$ @Qs	8.9317	1.98	0.067303
Nano- $\text{Fe}_3\text{O}_4$ @Qs/Ni (II)	3.1174	1.61	0.012749



**FIGURE 10** Photographs of aqueous suspension of nano- $\text{Fe}_3\text{O}_4$ @Qs/Ni (II) before (a) and after (b) magnetic capture

between aromatic ketones, aromatic amines, and aromatic aldehydes (Scheme 2).

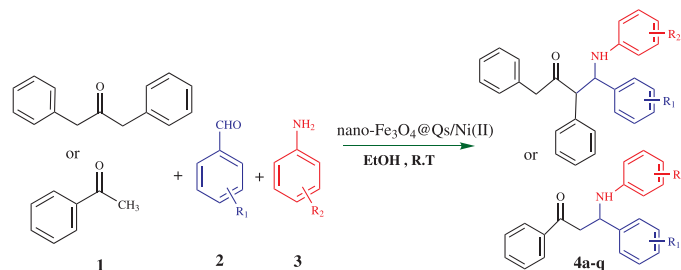
Initially, to optimize the reaction conditions reaction of acetophenone, benzaldehyde, and aniline was chosen as a model reaction. First, the model reaction was performed using nano- $\text{Fe}_3\text{O}_4$ , nano- $\text{Fe}_3\text{O}_4$ @Qs, or nano- $\text{Fe}_3\text{O}_4$ @Qs/Ni (II) as the catalyst. We found that nano- $\text{Fe}_3\text{O}_4$ @Qs/Ni (II) acted as a highly efficient catalyst for this reaction (Table 2, entry 5). Also, only a trace amount of the product was formed in the absence of a catalyst (Table 2, entry 1). Then the model reaction was carried out in various solvent with nano- $\text{Fe}_3\text{O}_4$ @Qs/Ni (II) as a catalyst at ambient temperature, and ethanol was recognized as the best solvent (Table 2, entry 5).

Afterward, optimization of catalyst amounts was carried out in the model study by using different amounts of the nano- $\text{Fe}_3\text{O}_4$ @Qs/Ni (II). The higher yield was obtained by increasing the amount of catalyst from 0.01 g to 0.1 g. However, further increase of the molar amount of the catalyst from 0.07 g to 0.1 g did not significantly increase the yield of the product (Table 2, entry4). Hence, the optimum concentration of nano- $\text{Fe}_3\text{O}_4$ @Qs/Ni (II) NPs was selected 0.07 in the model reaction. It was found that the best condition is using 0.07 g of the catalyst with ethanol at room temperature (Table 2, entry4).

The efficiency and generality of the reaction were investigated through various ketones, aromatic amines, and aldehydes. The results are summarized in Table 3.

The most probable mechanism for the synthesis of  $\beta$ -aminoketones was shown in Scheme 3.

Based on the results discussed before, it can be said that bonds between initially magnetic nano-catalyst and the carbonyl functional group of aldehyde (**2**) activate it for a nucleophilic rash toward amines (**3**), which leads intermediate (**5**) to be formed. Afterward, the intermediate loses a mole of water, and consequently, converts to imine (**6**). Then the enol, which has been formed via tautomerization of ketones (**1**) in the presence of nano-catalyst, reacts with imine. The fruit of the latest reaction is the final product (**4**) (Scheme 3).



**SCHEME 2** One-pot Mannich reaction of aromatic ketones, aromatic aldehydes and aromatic amines catalyzed by nano- $\text{Fe}_3\text{O}_4$ @Qs/Ni (II) at room temperature

**TABLE 2** The optimization of condition for the reaction of aniline, benzaldehyde and acetophenone

Entr	Catalyst(g)	Solvent-Temp(°C)	Time(h)	Yield (%) <sup>[a]</sup>
1	-	EtOH-Reflux	10	Trace
2	Nano-Fe <sub>3</sub> O <sub>4</sub> (0.1)	EtOH-Reflux	8	45
3	Nano-Fe <sub>3</sub> O <sub>4</sub> @QS(0.1)	EtOH-Reflux	6	75
4	Nano-Fe <sub>3</sub> O <sub>4</sub> @QS/Ni (II)(0.1)	EtOH-Reflux	4	91
5	Nano-Fe <sub>3</sub> O <sub>4</sub> @QS/Ni (II)(0.1)	EtOH-r.t.	4	93
6	Nano-Fe <sub>3</sub> O <sub>4</sub> @QS/Ni (II)(0.1)	MeOH-r.t.	5	65
7	Nano-Fe <sub>3</sub> O <sub>4</sub> @QS/Ni (II)(0.1)	CH <sub>3</sub> CN-r.t.	5	70
8	Nano-Fe <sub>3</sub> O <sub>4</sub> @QS/Ni (II)(0.1)	H <sub>2</sub> O-r.t.	5	Trace
9	Nano-Fe <sub>3</sub> O <sub>4</sub> @QS/Ni (II)(0.1)	HOAC-r.t.	5	55
10	Nano-Fe <sub>3</sub> O <sub>4</sub> @QS/Ni (II)(0.01)	EtOH-r.t.	4	55
11	Nano-Fe <sub>3</sub> O <sub>4</sub> @QS/Ni (II)(0.03)	EtOH-r.t.	4	70
12	Nano-Fe <sub>3</sub> O <sub>4</sub> @QS/Ni (II)(0.05)	EtOH-r.t.	4	85
13	Nano-Fe <sub>3</sub> O <sub>4</sub> @QS/Ni (II)(0.07)	EtOH-r.t.	4	93
14	Nano-Fe <sub>3</sub> O <sub>4</sub> @QS/Ni (II)(0.09)	EtOH-r.t.	4	93
15	Nano-Fe <sub>3</sub> O <sub>4</sub> @QS/Ni (II)(0.07)	EtOH-r.t.	2 2.30	93
16	Nano-Fe <sub>3</sub> O <sub>4</sub> @QS/Ni (II)(0.07)	EtOH-r.t.	2	89

<sup>a</sup>isolated Yield.**TABLE 3**  $\beta$ -aminoketone preparation by nano-Fe<sub>3</sub>O<sub>4</sub>@Qs/Ni (II)

Entry	ketone	R <sub>1</sub>	R <sub>2</sub>	Time (h)	Yield (%)	anti/syn	mp. (°C)	lit. mp. (°C)
<b>4a</b>	Acetophenone	H	H	2.30	93	-	164–165	165–168 <sup>[35]</sup>
<b>4b</b>	Acetophenone	4-OCH <sub>3</sub>	4-CH <sub>3</sub>	4	91	-	161–162	160–161 <sup>[36]</sup>
<b>4c</b>	Acetophenone	4-OCH <sub>3</sub>	H	3	90	-	167–168	165–168 <sup>[37]</sup>
<b>4d</b>	Acetophenone	H	4-Cl	2.30	93	-	171–172	170–171 <sup>[38]</sup>
<b>4e</b>	1,3-diphenylpropan-2-one	H	H	2.20	91	99/1	167–169	168–170 <sup>[39]</sup>
<b>4f</b>	1,3-diphenylpropan-2-one	4-F	H	2	82	91/9	46–148	148–150 <sup>[39]</sup>
<b>4j</b>	1,3-diphenylpropan-2-one	4-OCH <sub>3</sub>	H	3	84	99/1	131–133	132–133 <sup>[39]</sup>
<b>4 h</b>	Acetophenone	H	4-Br	2.30	95	-	177–179	[This work]
<b>4i</b>	Acetophenone	4-Cl	4-Br	2.40	90	-	171–173	[This work]
<b>4j</b>	Acetophenone	4-CH <sub>3</sub>	4-Br	3	88	-	175–177	[This work]
<b>4 k</b>	Acetophenone	4-CH <sub>3</sub>	4-NO <sub>2</sub>	3	86	-	163–165	[This work]
<b>4 l</b>	1,3-diphenylpropan-2-one	4-Br	H	2.30	85	92/8	124–126	[This work]
<b>4 m</b>	1,3-diphenylpropan-2-one	4-Cl	H	2.20	86	82/18	170–171	[This work]

Reaction conditions; aniline (1 mmol), aldehyde (1 mmol), acetophenon (1.1 mmol) or 1,3-diphenylpropan-2-one (1.1 mmol); catalyst (0.07 g).

## 5 | REUSABILITY AND LEACHING STUDY OF THE CATALYST

The most paramount feature of the novel catalyst is reusability. This feature was investigated in a model reaction of Acetophenone, Benzaldehyde, and aniline in optimization reaction conditions, after finished the reaction, the catalyst was separated via an external magnet.

The synthesized catalyst was washed with ethanol and then was dried at ambient temperature in vacuum condition. The wash and dry process were conducted four times. Then the washed sample was used in reaction cycles. As well-depicted in Figure 11, the catalyst is capable of being reused up to 4 runs to achieve a yield of 80 to 93%. Moreover, the ICP test results of virgin catalyst show that the concentration of Ni in the catalyst is

**SCHEME 3** Mechanism for formation of  $\beta$ -aminoketones in the presence of nano-Fe<sub>3</sub>O<sub>4</sub>@Qs/Ni (II)

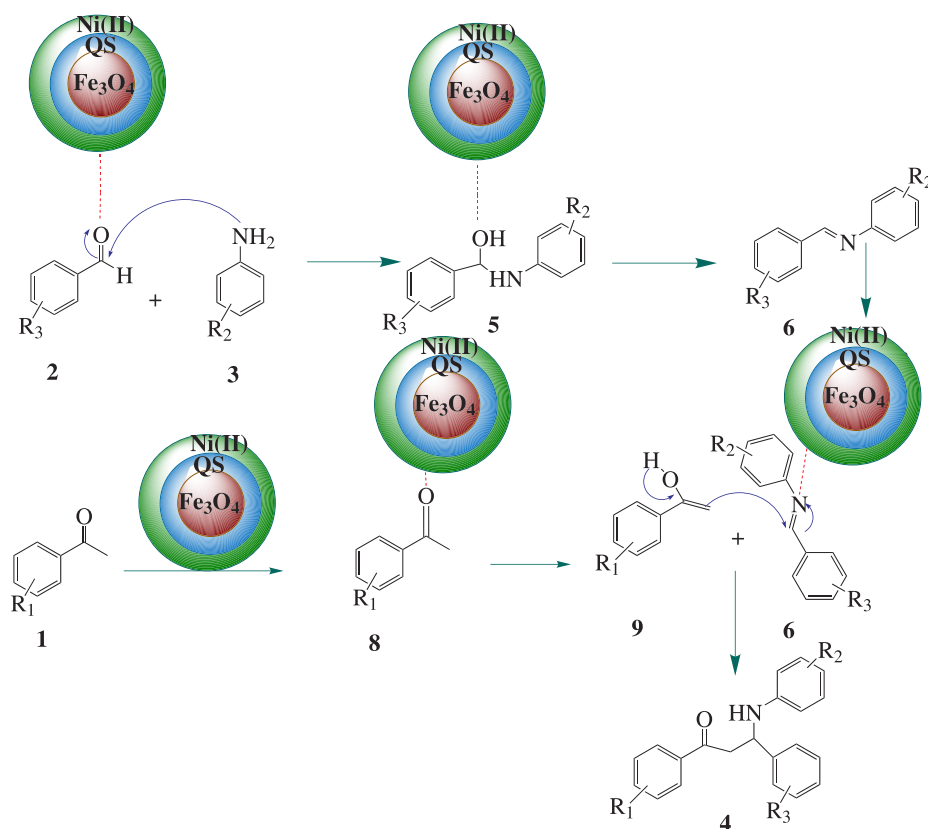
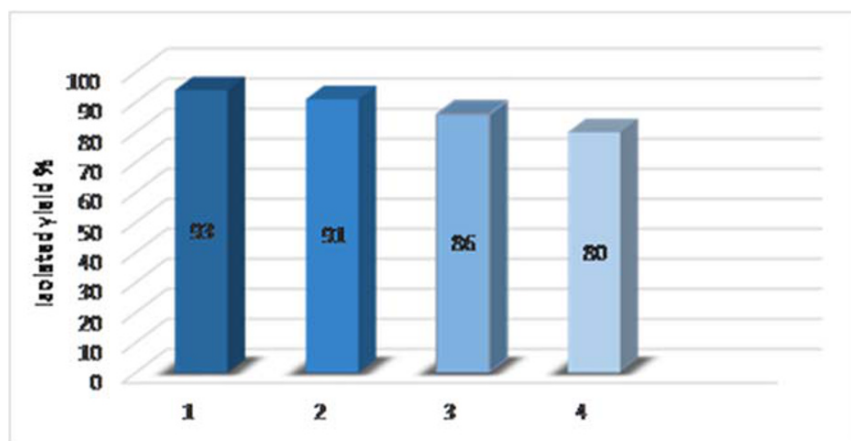


**FIGURE 11** The recycling experiment of nano-Fe<sub>3</sub>O<sub>4</sub>@Qs/Ni (II) in the synthesis of  $\beta$ -aminoketones reaction



$1.63 \times 10^{-3}$  mol/g. The same test was conducted on the recovered catalyst as well. It was disclosed that a very small amount of Ni molecules got lost after reaction because the Ni concentration in recovered catalyst decreased to  $1.63 \times 10^{-3}$ ,  $1.61 \times 10^{-3}$ ,  $1.6 \times 10^{-3}$ , and  $1.59 \times 10^{-3}$  mol/g after being recovered for first to fourth time, respectively.

Hot filtration experiment was conveyed in the coupling of 4-Bromoaniline 4-methyl benzaldehyde by acetophenone to examine the leaching of the catalyst. In this study, 49% of yield product was procured after a half-time reaction. Moreover, the same result was

achieved after the reaction half-time (90 min); in this way, the catalyst was recovered, and after filtration of the mixture, the reaction was to proceed until 3 hours (reaction ending time). It was observed that 50% of the product was yielded. As a result, these experiments validate that the synthesized catalyst is strong against leaching (Figure 11).

Finally, the efficiency and generality of this method were assessed by comparison with already synthesized catalysts. Comparison results are illustrated in Table 4. Based on the data shown in Table 4, nano-Fe<sub>3</sub>O<sub>4</sub>@Qs/Ni (II) is an efficient catalyst.

**TABLE 4** Efficiency comparison of nano-Fe<sub>3</sub>O<sub>4</sub>@Qs/Ni (II) with other catalysts

Entry	Catalyst	Amount	Temperature (°C)	Time(h)	yield (%) <sup>[b]</sup> Ref
1	BiNO <sub>3</sub>	10 mol%	25	4	89 <sup>[24]</sup>
2	Diaryliodonium (III)	10 mol%	25	24	83 <sup>[23]</sup>
3	Saccharose	15 mol%	25	9	92 <sup>[45]</sup>
4	Carbon-based solid acid	0.1 g	25	3.45	90 <sup>[22]</sup>
5	H <sub>3</sub> PW <sub>12</sub> O <sub>30</sub>	0.691 g	25	18	76 <sup>[21]</sup>
6	CFPIL-1	0.032 g	25	5	70 <sup>[31]</sup>
7	PS-SO <sub>3</sub> H	0.08 g	30	24	75 <sup>[46]</sup>
8	Al (CH <sub>3</sub> SO <sub>3</sub> ) <sub>3</sub> ·4H <sub>2</sub> O	0.5 mmol	25	8	86 <sup>[47]</sup>
9	[CellFemBen]CSA/EtOH	1.63 mol %	25	5	92 <sup>[48]</sup>
10	Citric acid	20 mol%	25	10	90 <sup>[25]</sup>
11	nano-Fe <sub>3</sub> O <sub>4</sub> @Qs/Ni (II)	0.07 g	25	2.30	93 [present work]

<sup>a</sup>Reaction conditions: benzaldehyde (1 mmol); aniline (1 mmol); acetophenone (1.1 mmol).

<sup>b</sup>Isolated yields.

## 6 | CONCLUSIONS

In summary, we have preparation and characterization of nano-Fe<sub>3</sub>O<sub>4</sub>@Qs/Ni (II) as a nanomagnetic catalyst for the synthesis of  $\beta$ -aminoketone derivatives via a one-pot three-component reaction of ketones, aromatic aldehydes, and aromatic amines in ethanol at room temperature. Fast reaction rate, good yields, and mild reaction conditions are the most significant advantages of this methodology. Furthermore, the catalyst can easily be separated and reused for more runs.

## ACKNOWLEDGEMENTS

All authors appreciate the laboratory facilities provided by Ahvaz Branch, Islamic Azad University, Ahvaz, Iran.

## ORCID

Hossein Anaraki-Ardakani  <https://orcid.org/0000-0002-0512-8033>

## REFERENCES

- [1] M. Chenguang, S. Hongqin, Z. Shixia, H. Peng, Z. Xiaoyan, C. Yun, L. Hongling, *J. Comp. Inter.* **2019**, 26, 537.
- [2] N. Mizuno, M. Misono, *Chem. Rev.* **1998**, 98, 199.
- [3] A. Y. Leung, *Encyclopedia of Common Natural Ingredients Used in Foods, Drugs, and Cosmetics*, Wiley, NY **1980**.
- [4] M. A. A. El-Remaily, A. M. Abu-Dief, *Tetrahedron* **2015**, 71, 2579.
- [5] M. A. A. El-Remaily, A. M. Abu-Dief, R. M. El-Khatib, *Appl. Organomet. Chem.* **2016**, 30, 1022.
- [6] A. M. Abu-Dief, I. F. Nassar, W. H. Elsayed, *Appl. Organomet. Chem.* **2016**, 30, 917.
- [7] A. A. Marzouk, A. M. Abu-Dief, A. A. Abdelhamid, *Appl. Organomet. Chem.* **2018**, 32, e3794.
- [8] X. Zheng, S. Luo, L. Zhang, J.-P. Cheng, *Green Chem.* **2009**, 11, 455.
- [9] Y. Jiang, C. Guo, H. Xia, I. Mahmood, C. Liu, H. Liu, *J. Mol. Catal. B: Enzym.* **2009**, 58, 103.
- [10] L. M. Rossi, N. J. S. Costa, F. P. Silva, R. Wojcieszak, *Green Chem.* **2014**, 6, 2906.
- [11] K. R. Rohit, M. R. Phadatarec, B. B. Sinha, D. M. Sakatee, A. V. Ghulef, G. S. Ghodake, N. G. Deshpandea, V. J. Fulari, *J. Taiwan Inst. Chem. Eng.* **2019**, 95, 357.
- [12] C. S. Gill, B. A. Price, C. W. Jones, *J. Catal.* **2007**, 251, 145.
- [13] P. V. Chavan, K. S. Pandit, U. V. Desai, M. A. Kulkarni, P. P. Wadgaonkar, *RSC Adv.* **2014**, 4, 42137.
- [14] A. Shaabani, A. Rahmati, Z. Badri, *Cat. Com.* **2008**, 1, 13.
- [15] M. Syamala, *Org. Prep. Proced. Int.* **2009**, 41, 1.
- [16] S. Balakrishnan, A. Rajendran, R. Kulandaivelu, S. Narayanan, T. S. Nellaiappan, *J. the Australian Cer. Soc.* **2019**, 55, 953.
- [17] Y. C. Teo, J. J. Lau, M. C. Wu, *Tetrahedron: Asymmetry* **2008**, 19, 186.
- [18] S. K. Aghdam, A. Moslemizadeh, M. Madani, M. Ghasemi, K. Shahbazi, M. K. Moraveji, *Chem. Eng. Res. Des.* **2019**, 147, 570.
- [19] A. Moslemizadeh, S. K. Aghdam, K. Shahbazi, S. Zendeheboudi, *J. Mol. Liq.* **2017**, 247, 269.
- [20] S. A. Soldatova, N. M. Kolyadina, A. T. Soldatenkov, A. V. Malkova, *Russ. J. Org. Chem.* **2019**, 55, 479.
- [21] N. Azizi, L. Torkiyan, M. R. Saidi, *Org. Lett.* **2006**, 8, 2079.
- [22] A. Davoodnia, A. Tavakoli-Nishaburi, N. Tavakoli-Hoseini, *Bull. Korean Chem. Soc.* **2011**, 32, 635.
- [23] Y. Zhang, J. Han, L. Zhen-Jiang, *RSC Adv.* **2015**, 5, 25485.
- [24] S. S. Mansoor, K. Aswin, K. Logaiya, S. P. N. Sudhan, *J. Saudi Chem. Soc.* **2015**, 19, 379.
- [25] V. B. Ningdale, U. N. Chaudhar, K. A. Shaikh, *J. Comp. Inter.* **2014**, 7, 86.
- [26] R. Duthaler, *Angew. Int. Ed. Engl.* **2003**, 42, 975.
- [27] A. Sasaoka, M. I. Uddin, A. Shimomoto, Y. Ichikawa, M. Shiro, H. Kotsuki, *Tetrahedron: Asymmetry* **2006**, 17, 2963.

- [28] E. Akceylan, M. Yilmaz, *Polycyclic Aromat. Compd.* **2016**, 36, 801.
- [29] S. A. A. Vandarkuzhali, B. Viswanathan, M. P. Pachamuthu, S. C. Kishore, *J. Inorganic and Organometallic Mater* **2020**, 30, 359.
- [30] T. P. Loh, S. C. Chen, *Org. Lett.* **2002**, 4, 3647.
- [31] A. G. Khiratkar, K. R. Balinge, K. J. Bhansali, P. R. Bhagat, *Res. Chem. Intermed.* **2018**, 44, 787.
- [32] X. Liu, Z. Ma, J. Xing, H. Liu, *J. Magn. Magn. Mater.* **2004**, 270, 1.
- [33] K. Ghodrati, E. Dezfoolnezhad, R. Badri, *New J. Chem.* **2016**, 40, 4575.
- [34] N. Kakesh, S. Sayyahi, R. Badri, *C. R. Chim.* **2018**, 21, 1023.
- [35] M. T. Maghsoodlou, N. Khorshidi, M. R. Mousavi, N. Hazeri, S. M. Habibi-khorassani, *Research on Chem Inter* **2014**, 41, 7497.
- [36] F. Dong, L. Jun, Z. Xin-Li, L. Zu-Liang, *Catal. Lett.* **2007**, 116, 76.
- [37] Y. Dai, B. D. Li, H. D. Quan, C. X. Lu, *Chin. Chem. Lett.* **2010**, 21, 31.
- [38] L. Wang, J. Han, J. Sheng, H. Tian, Z. Fan, *Cat. Com.* **2005**, 6, 201.
- [39] F. Nemati, A. S. Fakhaei, A. Amoozadeh, Y. Saeidi-Hayeniaz, *Synth. Commun.* **2011**, 41, 3695.
- [40] J. H. Jang, H. B. Lim, *Microchem. J.* **2010**, 94, 148.
- [41] A. M. Abu-Dief, M. S. Abdelbaky, D. Martinez-Blanco, Z. Amghouz, S. García-Granda, *Mater. Chem. Phys.* **2016**, 174.
- [42] E. M. M. Ibrahim, L. H. Abdel-Rahman, A. M. Abu-Dief, A. Elshafaiea, S. K. Hamdan, A. M. Ahmed, *Mater. Res. Bull.* **2018**, 99, 103.
- [43] W. S. Mohamed, M. Alzaid, M. S. M. Abdelbaky, Z. A. S. García-Grand, A. M. Abu-Dief, *Nanomaterials* **2019**, 9, 1602.
- [44] C. Toyos-Rodríguez, J. Calleja-García, L. Torres-Sánchez, A. López, A. M. Abu-Dief, A. Costa, L. Elbaile, R. D. Crespo, J. S. Garitaonandia, E. Lastra, J. A. García, F. J. García-Alonso, *J. Nanomaterials* **2019**, 10, Article ID 2464010.
- [45] M. R. Mousavi, N. Hazeri, M. T. Maghsoodlou, S. Salahi, S. M. Habibi-Khorassani, *Chin. Chem. Lett.* **2013**, 24, 411.
- [46] S. Iimura, D. Nobutou, K. Manable, S. Kobayashi, *Chem. Commun.* **2003**, 14, 1644.
- [47] M. Wang, Z.-G. Song, H. Jiang, *Org Prepa and Proce Intern* **2009**, 41, 315.
- [48] S. Khanapure, M. Jagadale, D. Kale, S. Gajare, G. Rashinkar, *Aust. J. Chem.* **2019**, 72, 513.

## SUPPORTING INFORMATION

Additional supporting information may be found online in the Supporting Information section at the end of this article.

**How to cite this article:** Heidarpour M, Anaraki-Ardakani H, Hasanzadeh N, Rayatzadeh A. Efficient synthesis of  $\beta$ -aminoketones catalyzed by  $\text{Fe}_3\text{O}_4@$  quillaja saponin/Ni (II) as a novel magnetic nano-catalyst. *Appl Organomet Chem.* 2020;e5834. <https://doi.org/10.1002/aoc.5834>